ChemComm

Chemical Communications

ROYAL SOCIETY OF CHEMISTRY
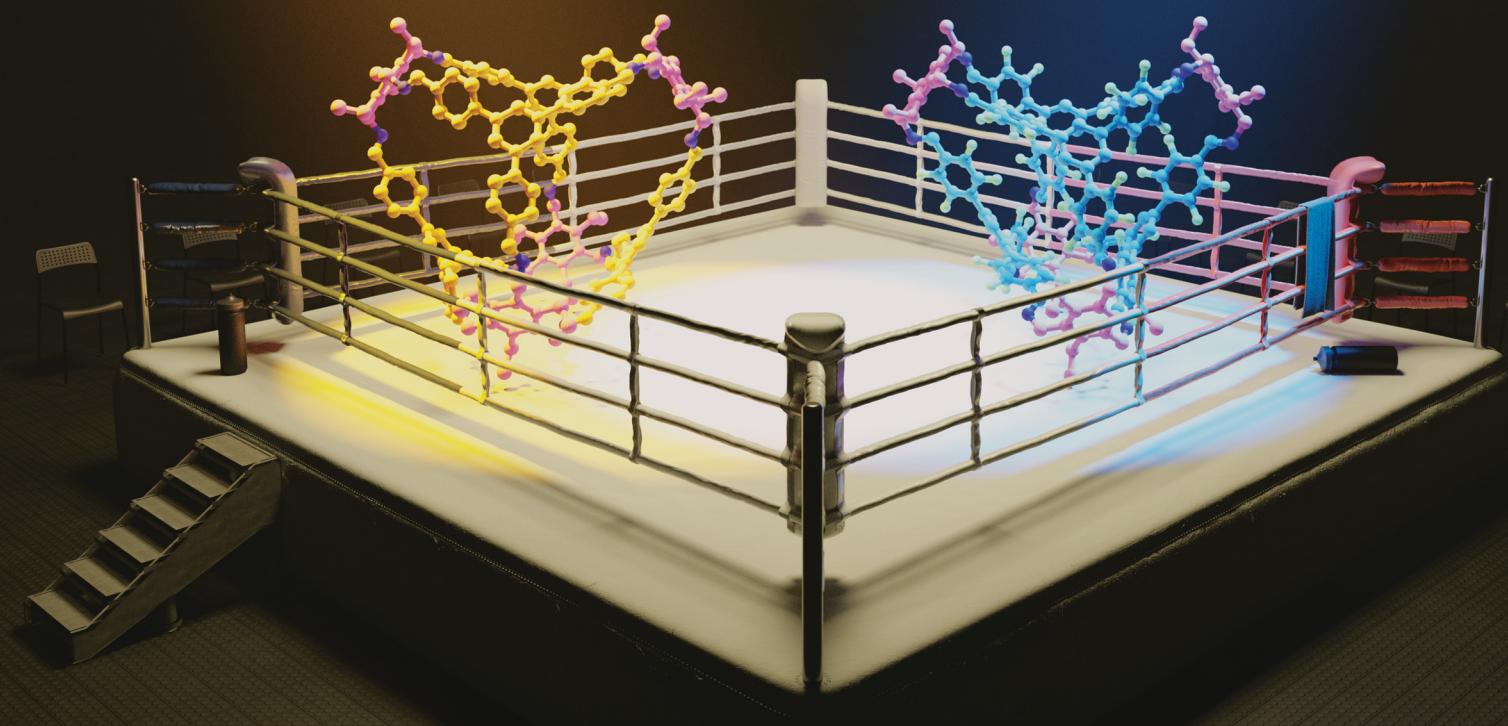
COMMUNICATION
Bernd M. Schmidt *et al.*
Fluorinated *vs.* non-fluorinated tetrahedral Tri^{4}Tri^4 porous organic cages for H$_2$, CO$_2$, and CH$_4$ adsorption

Fluorinated vs. non-fluorinated tetrahedral Tri⁴Tri⁴ porous organic cages for H_2, CO_2, and CH_4 adsorption†

Tim David, [a] Robert Oestreich, [b] Tobias Pausch, [a] Yuki Wada, [c] Tom Fleck-Kunde, [a] Masaki Kawano, [c] Christoph Janiak [b] and Bernd M. Schmidt [*a]

We present the synthesis of two porous complementary tetrahedral Tri⁴Tri⁴ imine cages, exhibiting Brunauer–Emmett–Teller (BET) surface areas of 591 $m^2 g^{-1}$ and 753 $m^2 g^{-1}$, suitable for the adsorption of H_2, CO_2, and CH_4. Comparisons in terms of crystallinity, thermal stability, porosity, and selectivity highlight the promising properties of fluorinated and non-fluorinated porous organic cages as functional materials.

Harnessing the power of organic synthesis in combination with subcomponent self-assembly of small and rigid building blocks into larger assemblies under thermodynamic control gives facile access to novel materials by molecular design.[1] Besides metal–organic frameworks (MOFs) and covalent organic frameworks (COFs), porous organic cages (POCs) are an emerging class of porous materials that are self-assembled in solution before precipitation as solid materials.[2] These discrete, three-dimensional molecular assemblies differ from networks by enabling straightforward solution-phase processing and analysis while also allowing post-synthetic transformations that can modify the scaffolds with atomic precision.[2,3] Dynamic covalent chemistry, particularly imine bond condensation[4] and boronate ester formation,[2a,b,e] among others,[2e] can be employed to access POCs. In comparison to imine cages, the rigidity of boronate ester linkages is beneficial for the synthesis of large shape-persistent cages,[2d–f] as shown by Mastalerz and co-workers, who reported a giant boronate ester cage with cuboctahedral symmetry exhibiting an extraordinarily

high surface area of SA_{BET} = 3758 $m^2 g^{-1}$ already in 2014, comparable to those observed for extended networks like MOFs and COFs.[5] The group of Beuerle recently reported the first water-stable boronate ester cage,[6] stable under ambient conditions with a well-defined microporous solid state structure (SA_{BET} = 2534 $m^2 g^{-1}$), paving the way for further applications of dynamic covalent boronate ester materials.[7] In addition, the use of computational crystal structure prediction,[8] along with computational design in supramolecular synthesis at both the molecular level and in the solid state,[9] has been key to obtaining a complex, shape-persistent [4[2+3]+6] cage by reversible nucleophilic aromatic substitution.[10] From the various accessible cage structures, the class of Tri⁴Tri⁴ cages surprisingly remains largely underrepresented. Despite their tetrahedral structure enabling the formation of three-dimensional pores, only a few porous cages have been reported to date.[9,11a–c,12]

Herein, we present the synthesis of two highly porous Tri⁴Tri⁴ imine cages, **Et⁴H⁴** and **Et⁴F⁴**. When reacting the pre-organised 1,3,5-tris(aminomethyl)-2,4,6-triethylbenzene (**Et**) with the non-fluorinated trialdehyde (**H**) and the analogous highly fluorinated trialdehyde (**F**), **Et⁴H⁴** and **Et⁴F⁴** form, respectively, opening up the possibility to investigate the influence of fluorinated units in porous organic materials (Fig. 1a). Heating the building blocks in a chloroform/methanol (3 : 1) mixture at 60 °C without stirring results in the growth of cube-like crystals on the walls of the reaction vessel. Repeated solvent exchange against *n*-pentane and drying of the crystals in air gives **Et⁴H⁴** in 84% and **Et⁴F⁴** in 45% yield as colourless crystals (Fig. S9–S14, ESI†). The ¹H NMR analysis of the redissolved crystals shows sharp signals, indicating the clean formation of both cages (Fig. 1b). Furthermore, ¹⁹F NMR analysis of **Et⁴F⁴** reveals only one broad signal for the two independent aromatic fluorine atoms (Fig. S44, ESI†). Size determination using ¹H DOSY experiments gives solvodynamic radii of r_{solv} = 1.04 nm ($D = 3.98 \times 10^{-10} m^2 s^{-1}$ in CDCl₃) for **Et⁴H⁴** and r_{solv} = 1.24 nm ($D = 3.35 \times 10^{-10} m^2 s^{-1}$ in CDCl₃) for **Et⁴F⁴**, respectively (Fig. S1–S4, ESI†). Crystals suitable for single-crystal X-ray diffraction (SC-XRD) analysis can be obtained directly from the reaction mixture and reveal the cubic space groups *F*43*c* for **Et⁴H⁴**

ᵃ Institut für Organische Chemie und Makromolekulare Chemie, Heinrich-Heine-Universität Düsseldorf, Universitätsstraße 1, 40225 Düsseldorf, Germany.
E-mail: bernd.schmidt@hhu.de

ᵇ Institut für Anorganische Chemie und Strukturchemie, Heinrich-Heine-Universität Düsseldorf, Universitätsstraße 1, 40225 Düsseldorf, Germany

ᶜ Department of Chemistry, School of Science, Institute of Science Tokyo, 2-12-1 Ookayama, Meguro-ku, Tokyo 152-8550, Japan
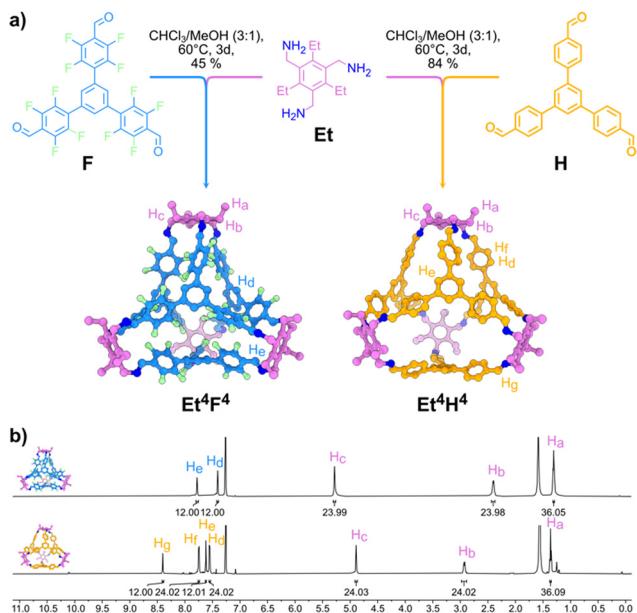
Fig. 1 (a) Synthesis of crystalline **Et⁴F⁴** and **Et⁴H⁴** by combining **H** and **F** with 1.20 eq. **Et**, respectively; (b) ^{1}H NMR spectra of **Et⁴F⁴** and **Et⁴H⁴** recorded in CDCl₃ at 25 °C.

and $Fd3$ for **Et⁴F⁴**. **Et⁴F⁴** assembles in a face-to-face arrangement with centroid-to-centroid distances of 4.5 Å for the fluorinated tetraphenyl panels packing loosely and C–H⋯F contacts between the inner fluorine and the hydrogen of the phenyl core of a neighbouring cage's panel with a distance of 3.1 Å, resulting in interconnected windows and a three-dimensional pore network (Fig. S6, ESI†). Additional vertex-to-vertex arrangements of **Et** from four separate cages lead to isolated extrinsic pores that are inaccessible. In contrast, **Et⁴H⁴** packs in a close window-to-window arrangement but also exhibits an extensively connected three-dimensional pore network. Powder X-ray diffraction (PXRD) analysis of dried cage crystals shows sharp diffraction for **Et⁴F⁴**, revealing a partly crystalline material before and after all gas sorption experiments (Fig. 2a). Whereas the PXRD analysis of **Et⁴H⁴** shows broad diffraction, indicating the formation of a largely amorphous material upon activation (Fig. 2a). Additional thermogravimetric analysis shows a high thermal stability for both materials, with decomposition temperatures of 348 °C for **Et⁴F⁴** and 352 °C for **Et⁴H⁴**, respectively (Fig. S21 and S22, ESI†). **Et⁴F⁴**'s seemingly more robust networked cages and high thermal stability are most likely the result of several stabilising weak interactions between the fluorinated and (non-)fluorinated parts of the cages in the highly symmetric lattice.[13] Jiang *et al.* outlined the improved crystallinity of fluorine-containing systems due to self-complementary electronic interactions between fluorinated and non-fluorinated counterparts.[14,15] The pore sizes of **Et⁴H⁴** range from 5.6 Å to 11.7 Å, derived from the SC-XRD data. Analogues are the diameters 3.4 Å and 6.4 Å for **Et⁴F⁴**, respectively. Non-local density functional theory (NLDFT) and grand canonical Monte Carlo (GCMC) calculations based on the N₂ sorption isotherms at 77 K also show the smaller pore size of **Et⁴F⁴** with a narrow pore size distribution around 5.8 Å (Fig. S29,

ESI†). Contrarily, the pore size distribution of **Et⁴H⁴** shows a broader maximum for micropores around 14 Å and some mesopores with pore diameters between 20 Å and 80 Å, which are larger than the cage compounds themselves (Fig. S26, ESI†), indicating cracks and a subsequent loss of crystallinity. This suggests that the solvent exchange and subsequent drying of the crystals obtained from the reaction mixture, in contrast to **Et⁴F⁴**, leads to a loss of crystallinity for **Et⁴H⁴**. The observed porosity of **Et⁴H⁴**, however, is suggested to be caused by the cage's large voids in the amorphous material. The pore widths of both cages and the kinetic diameters of H₂ (2.89 Å), CO₂ (3.30 Å), and CH₄ (3.80 Å) indicate that both should be suitable for the adsorption of these gases.[16] Therefore, the dried crystals were activated by heating under dynamic vacuum overnight, at 80 °C for **Et⁴F⁴** and at 140 °C for **Et⁴H⁴**. Between the measurements, both samples were recycled by heating to 80 °C for two hours *in vacuo*. The obtained specific surface areas (SA) of 591 m² g⁻¹ and 753 m² g⁻¹ for **Et⁴F⁴** and **Et⁴H⁴**, respectively, determined by the BET method, are comparable to the Tri²Di⁶ cage **CC3** (SA$_{BET}$ = 624 m² g⁻¹) and a Tri²Di³ *exo*-functionalised salicylimine cage (SA$_{BET}$ = 744 m² g⁻¹) of similar sizes.[17,18] To the best of our knowledge, **Et⁴F⁴** and **Et⁴H⁴** exhibit among the largest specific surface areas reported for tetrahedral Tri⁴Tri⁴ cages. **Et⁴F⁴** is additionally the largest fluorinated Tri⁴Tri⁴ imine cage, surpassing cage **FC1** (SA$_{BET}$ = 536 m² g⁻¹) previously published by our group.[12] The pore volume of both cages was determined from the N₂ sorption isotherms at 77 K by GCMC as well as NLDFT calculations, revealing a total pore volume of 0.39 cm³ g⁻¹ and a micropore volume of 0.21 cm³ g⁻¹ for **Et⁴F⁴** and 0.59 cm³ g⁻¹ and 0.24 cm³ g⁻¹ for **Et⁴H⁴**, respectively. The **Et⁴H⁴** cage adsorbs 14.5 mmol g⁻¹ (28.9 wt%) of N₂ at 77 K and 0.95p/p_0 (Fig. 2c), as beyond this relative pressure, N₂ condensation inside the pore network can be observed, which is often not considered. This is comparable to the adsorption performance of the substituted Tri⁴Di⁶ cages reported by Mastalerz *et al.*, which also remain porous in their amorphous state while exhibiting specific surface areas ranging from 690 to 727 m² g⁻¹, with N₂ uptake values between 17.4 and 21.4 mmol g⁻¹ at 77 K and 0.95p/p_0 bar.[19] The N₂ sorption isotherm of **Et⁴H⁴** can be classified as a combination of type-Ib (low p/p_0 for the microporous region) and a type-II isotherm (higher p/p_0, macroporous multi-layer region) with a wide H4 hysteresis loop.[20] **Et⁴F⁴** exhibits a higher gas uptake of 10.1 mmol g⁻¹ (22.0 wt%) N₂ at 77 K and 0.95p/p_0 (Fig. 2c), compared to the slightly larger **CC3** (8.2 mmol g⁻¹, 18.6 wt%, 1 bar).[17] The N₂ adsorption isotherm can again be described as a combination of a type-I and type-II isotherm with a H4 hysteresis loop. Noteworthy is the step in the H4 hysteresis loop at 0.5p/p_0, more clearly seen in **Et⁴F⁴** than in **Et⁴H⁴**, which we assign to two types of bottle-neck pores in combination with framework reconstruction.[20] Exhibiting a hydrogen uptake of 6.1 mmol g⁻¹ (1.2 wt%), **Et⁴H⁴** adsorbs more H₂ at 77 K and 1 bar than the almost twice as large Tri⁴Di⁶ *tert*-butyl substituted adamantoid cage (SA$_{BET}$ = 1377 m² g⁻¹, 5.6 mmol g⁻¹) and is also comparable to the smaller sized **CC2** (SA$_{BET}$ = 533 m² g⁻¹, 5.9 mmol g⁻¹) and **CC3** (SA$_{BET}$ = 624 m² g⁻¹, 5.0 mmol g⁻¹) POCs reported.[17,21] We further measured an adsorption of 3.0 mmol g⁻¹ (11.8 wt%) for
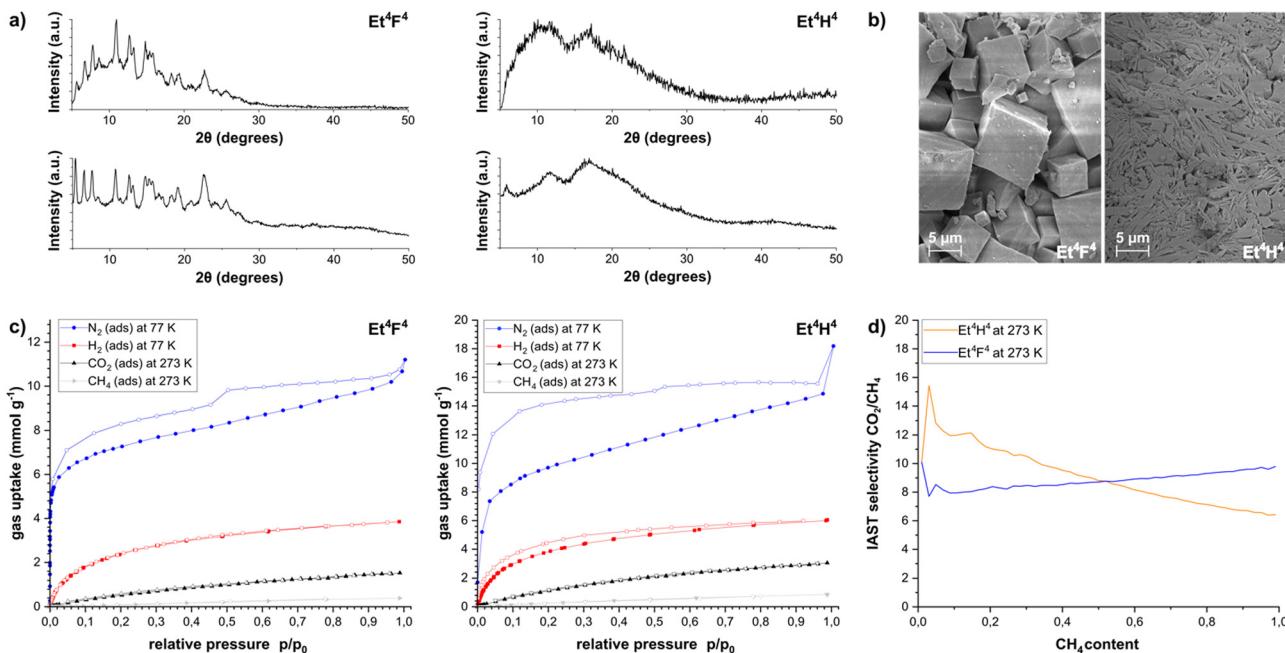
Fig. 2 (a) Powder X-ray diffraction (PXRD) patterns before (bottom) and after (top) sorption experiments of Et^4F^4 (left) and Et^4H^4 (right); (b) true to scale cutouts from scanning electron microscope (SEM) images of Et^4F^4 (left) and Et^4H^4 (right), scanning voltage 5 kV; (c) gas adsorption (filled) and desorption (hollow) overview of Et^4F^4 (left) and Et^4H^4 (right); (d) ideal adsorbed solution theory (IAST) selectivity curves of Et^4F^4 (orange) and Et^4H^4 (blue) for varying gas compositions of CO_2/CH_4 (1 bar total pressure, 273 K).

CO_2 at 273 K and 1 bar. This value is again well comparable with the cages mentioned above showing CO_2 uptakes of 2.7 mmol g^{-1} (11.8 wt%), 3.0 mmol g^{-1} (11.7 wt%), and 2.5 mmol g^{-1} (9.9 wt%), respectively.[17,22] For CH_4, we measured a low gas uptake at 273 K and 1 bar of 0.8 mmol g^{-1} (1.3 wt%) compared to **CC2** (1.1 mmol g^{-1}, 1.7 wt%) and **CC3** (1.5 mmol g^{-1}, 2.3 wt%), resulting in a higher selectivity of 10.3 : 1 (w/w) for CO_2 over CH_4, which is well comparable to the selectivity of 10 : 1 (w/w) for the adamantoid cage by Mastalerz *et al.*[17,21] The measured gas adsorptions of the highly fluorinated Et^4F^4 are much lower than for the non-fluorinated Et^4H^4. Et^4F^4 adsorbs at 1 bar 3.9 mmol g^{-1} (0.8 wt%) H_2 (77 K), 1.5 mmol g^{-1} (6.3 wt%) CO_2 (273 K), and 0.4 mmol g^{-1} (0.6 wt%) CH_4 (273 K). The smaller, previously reported cage **FC1** exhibits higher adsorption properties for H_2 (7.5 mmol g^{-1} and 1.5 wt%) and CO_2 (4.2 mmol g^{-1} and 19.0 wt%) than both here reported cages.[12] To date, **FC1** is the cage with the highest CO_2 uptake ever reported for POCs.[10] When calculating the gas uptake for a porous material in moles of gas per gramme material, the molecular weight and density of the material are not taken into account. This entails that smaller cages, such as **FC1** (1309 g mol^{-1}), frequently display higher gas uptakes since there are essentially more cage molecules with specific surface area per gramme of material available. To evaluate the quantitative uptake, we also calculated the gas uptake in moles of gas per mole of cage and volume of adsorbed gas per volume of the cage (Tables S3–S5, ESI†). For CO_2, we calculated gas uptakes of 5.5 mol mol^{-1} for **FC1** and 4.9 mol mol^{-1} together with 7.1 mol mol^{-1} for Et^4F^4 and Et^4H^4, respectively. In this regard, Et^4H^4 is the superior adsorbent material in direct comparison to **FC1**. With increasing pore sizes, the number of adsorbed gas molecules that directly interact with

the surface area becomes less, and therefore higher relative pressure is needed for the pore filling through multilayer adsorption by adsorbate–adsorbate interactions to achieve a higher gas uptake. However, besides adsorption capacity, selectivity is arguably another critical property of a porous material for industrial applications such as gas purification.[23] Natural gas, primarily composed of CH_4, is a crucial energy source that is often contaminated with over 40% N_2 and CO_2, which must be removed before combustion.[24] Therefore, we calculated the ideal adsorbed solution theory (IAST) selectivity for CO_2 over CH_4, based on the sorption isotherms at 273 K and 1 bar (Fig. 2d). For a 1 : 1 $CO_2 : CH_4$ composition, both cages exhibit nearly the same selectivity (8.80 and 8.71 for Et^4H^4 and Et^4F^4, respectively). With decreasing CO_2 content, the selectivity of the non-fluorinated cage decreases to 6.6 at 95% CH_4 in the gas composition, whereas the selectivity of the fluorinated cage increases to 9.7 for the identical composition (Fig. 2d). In addition to the recent studies of our group, Miljanić *et al.* reported the higher selectivity of fluorinated covalent triazine frameworks to CO_2 in a CH_4-enriched composition and the higher CO_2-phillicity of fluorine-containing materials, resulting from attractive quadrupole interactions.[12,13b] The better selectivity of Et^4F^4, especially in CH_4-enriched compositions ($\geq$60%), shows the potential for the application of fluorinated materials in the purification of gases.

In conclusion, we presented the successful synthesis and characterisation of two new porous Tri^4Tri^4 imine cages, Et^4H^4 and the highly fluorinated Et^4F^4. To the best of our knowledge, both cages are among the largest shape-persistent cages within this topology.[11a–c,12] We further investigated the influence of the incorporation of highly fluorinated building blocks into

porous materials in terms of retention of crystallinity, thermal stability, porosity, selectivity, and reusability. The fluorinated **Et⁴F⁴** shows a much higher retention of the crystallinity, whereas **Et⁴H⁴** was obtained as an amorphous material upon solvent removal. Both materials exhibit high thermal stability of approximately 350 °C and gas adsorption measurements further demonstrated that both cages are highly porous with BET surface areas of 591 m^2 g^{-1} (**Et⁴F⁴**) and 753 m^2 g^{-1} (**Et⁴H⁴**), which are accessible for the uptake of H_2 and CO_2, simultaneously showing a low affinity towards CH_4. At 273 K and 1 bar, both cages nearly exhibit the same IAST selectivity for CO_2 over CH_4 for a 1 : 1 composition of the gases of 8.8 and 8.7 for **Et⁴H⁴** and **Et⁴F⁴**, respectively. For compositions with decreasing amounts of CO_2, the selectivity for CO_2 of the non-fluorinated cage decreases, whereas the selectivity of the fluorinated cage increases, demonstrating the advantages of fluorine-containing building blocks in materials for gas purification. Unveiling significant relationships between the structural and electronic differences of fluorinated and non-fluorinated building blocks, offering new ways to tailor highly selective porous organic architectures for advanced functional materials.

Data availability

The data supporting this article have been included as part of the ESI.† Crystallographic data for has been deposited at the CCDC under 2388131 (**Et⁴F⁴**) and 2388132 (**Et⁴H⁴**) and can be obtained from https://www.ccdc.cam.ac.uk/structures/.

Conflicts of interest

There are no conflicts to declare.

References

1 (a) F. B. L. Cougnon, A. R. Stefankiewicz and S. Ulrich, *Chem. Sci.*, 2024, **15**, 879; (b) E. Busseron, Y. Ruff, E. Moulin and N. Giuseppone, *Nanoscale*, 2013, **5**, 7098.
2 (a) S. Ivanova and F. Beuerle, *Isr. J. Chem.*, 2024, **64**, e202400025; (b) T. Kunde, T. Pausch and B. M. Schmidt, *Eur. J. Org. Chem.*, 2021, 5844; (c) X. Zhang, Z. Chen, X. Liu, S. L. Hanna, X. Wang, R. Taheri-Ledari,

A. Maleki, P. Li and O. K. Farha, *Chem. Soc. Rev.*, 2020, **49**, 7406; (d) M. Mastalerz, *Acc. Chem. Res.*, 2018, **51**, 2411; (e) F. Beuerle and B. Gole, *Angew. Chem., Int. Ed.*, 2018, **57**, 4850; (f) T. Hasell and A. I. Cooper, *Nat. Rev. Mater*, 2016, **1**, 16053.
3 (a) M. Yang, K. Su and D. Yuan, *Chem. Commun.*, 2024, **60**, 10476; (b) T. Pausch, T. David, T. Fleck-Kunde, H. Pols, J. Gurke and B. M. Schmidt, *Angew. Chem., Int. Ed.*, 2024, **63**, e202318362; (c) H. Wang, Y. Jin, N. Sun, W. Zhang and J. Jiang, *Chem. Soc. Rev.*, 2021, **50**, 8874.
4 K. Acharyya and P. S. Mukherjee, *Angew. Chem., Int. Ed.*, 2019, **58**, 8640.
5 G. Zhang, O. Presly, F. White, I. M. Oppel and M. Mastalerz, *Angew. Chem., Int. Ed.*, 2014, **53**, 1516.
6 P. H. Kirchner, L. Schramm, S. Ivanova, K. Shoyama, F. Würthner and F. Beuerle, *J. Am. Chem. Soc.*, 2024, **146**, 5305.
7 (a) S. Ivanova, E. Köster, J. J. Holstein, N. Keller, G. H. Clever, T. Bein and F. Beuerle, *Angew. Chem., Int. Ed.*, 2021, **60**, 17455; (b) S. Klotzbach, T. Scherpf and F. Beuerle, *Chem. Commun.*, 2014, **50**, 12454.
8 R. L. Greenaway, V. Santolini, A. Pulido, M. A. Little, B. M. Alston, M. E. Briggs, G. M. Day, A. I. Cooper and K. E. Jelfs, *Angew. Chem., Int. Ed.*, 2019, **58**, 16275.
9 (a) A. R. Basford, S. K. Bennett, M. Xiao, L. Turcani, J. Allen, K. E. Jelfs and R. L. Greenaway, *Chem. Sci.*, 2024, **15**, 6331; (b) A. Tarzia, E. H. Wolpert, K. E. Jelfs and G. M. Pavan, *Chem. Sci.*, 2023, **14**, 12506; (c) V. Santolini, M. Miklitz, E. Berardo and K. E. Jelfs, *Nanoscale*, 2017, **9**, 5280.
10 Q. Zhu, H. Qu, G. Avci, R. Hafizi, C. Zhao, G. M. Day, K. E. Jelfs, M. A. Little and A. I. Cooper, *Nat. Synth.*, 2024, **3**, 825.
11 (a) J. C. Lauer, W.-S. Zhang, F. Rominger, R. R. Schröder and M. Mastalerz, *Chem. – Eur. J.*, 2018, **24**, 1816; (b) K. Tian, X. Wang, M. P. Schuldt, S. M. Elbert, F. Rominger and M. Mastalerz, *Org. Mater.*, 2023, **5**, 91; (c) S. M. Elbert, F. Rominger and M. Mastalerz, *Chem. Eur. J.*, 2014, **20**, 16707.
12 T. Kunde, E. Nieland, H. V. Schröder, C. A. Schalley and B. M. Schmidt, *Chem. Commun.*, 2020, **56**, 4761.
13 (a) Z. Zhang and O. Š. Miljanić, *Org. Mater.*, 2019, **1**, 19; (b) Z. Yang, S. Wang, Z. Zhang, W. Guo, K. Jie, M. I. Hashim, O. Š. Miljanić, D.-E. Jiang, I. Popovs and S. Dai, *J. Mat. Chem. A*, 2019, **7**, 17277; (c) T.-H. Chen, I. Popov, W. Kaveevivitchai, Y.-C. Chuang, Y.-S. Chen, A. J. Jacobson and O. Š. Miljanić, *Angew. Chem., Int. Ed.*, 2015, **54**, 13902; (d) T.-H. Chen, I. Popov, W. Kaveevivitchai, Y.-C. Chuang, Y.-S. Chen, O. Daugulis, A. J. Jacobson and O. Š. Miljanić, *Nat. Commun.*, 2014, **5**, 5131.
14 X. Chen, M. Addicoat, S. Irle, A. Nagai and D. Jiang, *J. Am. Chem. Soc.*, 2013, **135**, 546.
15 B. M. Schmidt, A. K. Meyer and D. Lentz, *CrystEngComm*, 2017, **19**, 1328.
16 N. Mehio, S. Dai and D.-E. Jiang, *J. Phys. Chem. A*, 2014, **118**, 1150.
17 T. Tozawa, J. T. A. Jones, S. I. Swamy, S. Jiang, D. J. Adams, S. Shakespeare, R. Clowes, D. Bradshaw, T. Hasell, S. Y. Chong, C. Tang, S. Thompson, J. Parker, A. Trewin, J. Bacsa, A. M. Z. Slawin, A. Steiner and A. I. Cooper, *Nat. Mater.*, 2009, **8**, 973.
18 M. W. Schneider, I. M. Oppel and M. Mastalerz, *Chem. – Eur. J.*, 2012, **18**, 4156.
19 M. W. Schneider, I. M. Oppel, H. Ott, L. G. Lechner, H.-J. S. Hauswald, R. Stoll and M. Mastalerz, *Chem. – Eur. J.*, 2012, **18**, 836.
20 K. Kaneko, A. V. Neimark, J. P. Olivier, F. Rodriguez-Reinoso, J. Rouquerol, K. S. W. Sing and M. Thommes, *Pure Appl. Chem.*, 2015, **87**, 1051.
21 M. W. Schneider, I. M. Oppel, O. Presly and M. Mastalerz, *Angew. Chem., Int. Ed.*, 2011, **50**, 1046.
22 M. W. Schneider, I. M. Oppel, A. Griffin and M. Mastalerz, *Angew. Chem., Int. Ed.*, 2013, **52**, 3611.
23 (a) L. Yu, L. Hao, C. Zhang, L. Qiao, J. Pang, H. Wang, H. Chang, W. Fan, R. Wang, D. Sun, L. Fan and Z. Kang, *J. Membr. Sci.*, 2024, **711**, 123231; (b) G. Wu, J.-R. Wu, Y. Wang and Y.-W. Yang, *Chem.*, 2009, **9**, 2918.
24 J. R. Long, D. M. D'Alessandro and B. Smit, *Angew. Chem., Int. Ed.*, 2010, **49**, 6058.